Nanoporous Metals by Alloy Corrosion: Formation and Mechanical Properties

Jörg Weissmüller, Roger C. Newman, Hai-Jun Jin, Andrea M. Hodge, and Jeffrey W. Kysar

Abstract

Nanoporous metals prepared by the corrosion of an alloy can take the form of monolithic, millimeter-sized bodies containing approximately 10^{15} nanoscale ligaments per cubic millimeter. The ligament size can reach down to the very limits of stability of nanoscale objects. The processes by which nanoporous metals are formed have continued to be fascinating, even though their study in relation to surface treatment, metal refinement, and failure mechanisms can be traced back to ancient times. In fact, the prospect of using alloy corrosion as a means of making nanomaterials for fundamental studies and functional applications has led to a revived interest in the process. The quite distinct mechanical properties of nanoporous metals are one of the focus points of this interest, as relevant studies probe the deformation behavior of crystals at the lower end of the size scale. Furthermore, the coupling of bulk stress and strain to the forces acting along the surface of nanoporous metals provide unique opportunities for controlling the mechanical behavior through external variables such as the electrical or chemical potentials.

Introduction

Condensed matter may exhibit porosity in a variety of expressions.[1] Some substances (e.g., zeolites) will spontaneously form crystalline structures with regular arrays of interstices. Others, such as bone, are formed by biological growth or by more or less random agglomeration of objects, either controlled by the kinetics of aggregation, as in granular matter, or by minimization of their energy (e.g., capillary energy), as in foams. There are many other processes that lead to the formation of porous matter, and expressions of porosity are ubiquitous in many branches of science, including hard and soft condensed matter sciences, materials sciences, and life sciences.

The class of porous materials that are of interest in the present article are formed by the combined processes of (1) the selective removal of atoms of one species from a solid solution—forming random porosity at an atomic scale, and (2) the rearrangement—at the scale of a few nanometers—of the resulting atomic-scale mixture of interstitials and atoms of the remaining species into two phases, solid and void, that are separated by an interface. Typically, the microstructural length scales associated with the two phases, pores and solid "ligaments," are both on the order of few nanometers. Our interest in these objects relates directly to the formation mechanism: it is a particularly well-defined example of the nonequilibrium, driven processes that are also relevant to current issues in fields such as materials behavior under irradiation, mechanical alloying, spinodal decomposition, and self-organization.[2] The structure sizes of interest—nanometers—are large enough to suggest a description of these "nanoporous materials" in terms of classical, continuum approaches in thermodynamics and mechanics, including the separation into bulk properties and capillary terms. The microstructural length scales are, on the other hand, small enough to expose a wide range of new phenomena that are characteristic of nanoscale matter, such as truly interface-controlled materials behavior or size effects on their properties.

The characteristic pore or ligament size in nanoporous metals formed by alloy corrosion can, in fact, be tuned down to a few nanometers. Even though the microstructural scale may reach down to fundamental lower size limits for stable states of crystalline matter, the samples are typically monolithic macroscopic bodies, as exemplified in Figure 1. Alternatively, alloy corrosion is readily combined with thin film deposition and lithographic processes, allowing porous metal elements to be implemented in possible devices in microelectronics, micromechanics, or photonics applications.

One of the distinguishing features of nanoporous solids formed by alloy corrosion is their bicontinuous microstructure, with two contiguous and interpenetrating phases. The transmission electron microscopy (TEM) images in Figure 1a and 1b illustrate this geometry. When at least one of the phases—for instance, a gas in the void space—allows the fast transport of a signal, then the interfaces can be addressed and their properties manipulated. That predestines nanoporous solids as objects of study for a new class of functional materials, in which interfacial behavior is controlled reversibly by external variables, and the entire material reacts.[3] Recent suggestions of nanoporous solids for electrochemical[4] or chemical[5] actuation or as tunable conductors[6,7] or magnets[8,9] exemplify this concept. Other suggested or emerging applications, specifically in catalysis, are reported in the article by Ding and Chen in this issue. Any suggested application of such materials will first and foremost require two important issues to be understood: the making of a high-quality porous material and the retention of its structural integrity under the action of mechanical load. This article aims to summarize our understanding of these two issues.

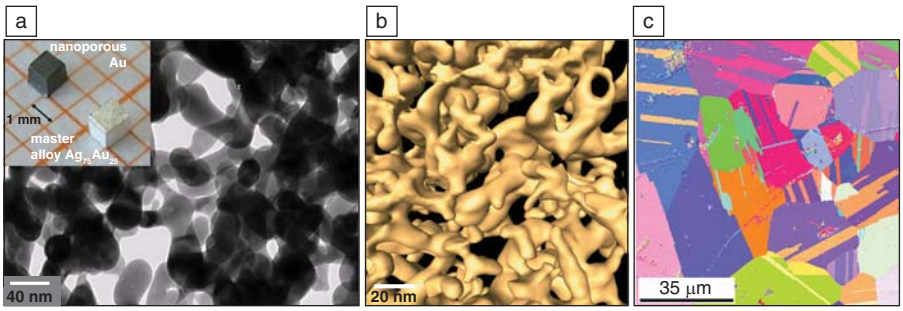

Figure 1. Length scales in nanoporous materials. While samples can take the form of monolithic bodies of macroscopic size, their microstructure consists of ligaments that can reach down to few nanometers. (a) Bright-field transmission electron microscope (TEM) image of a nanoporous gold (NPG) sample. Inset: photograph showing a millimeter-sized master alloy and a bulk dealloyed NPG sample containing about 10^{15} ligaments around 10 nm in size.[46] (b) 3D reconstruction of NPG obtained by electron tomography in a TEM.[49] (c) Electron backscatter diffraction image showing a micron-sized grain structure of NPG.[47]

Alloy Corrosion

Dealloying is the selective electrolytic dissolution of a less-noble element from a metallic solid solution or intermetallic compound, leaving a nanoporous residue (see Ding and Chen article in this issue for more details). Dealloying is an ancient technology and was used by several civilizations to gild the surfaces of objects that were made mainly of copper and/or silver. This generally involved the application of heat as well as chemical attack. There appears to have been a spectrum of techniques, ranging from true dealloying to a cycle of alternate dry oxidation and aqueous oxide dissolution. Dealloying was also used for a more macroscopic separation or "parting" of gold from alloys with copper and/or silver. Eventually nitrate environments were preferred; there are several different recipes in the Codex Atlanticus (ca. 1508) using saltpeter (potassium nitrate)[10], and since then, nitric acid has been the preferred reagent.[11]

The key discovery about "parting" was that the less-noble metal or metals had to be present above a certain percentage, or parting limit, otherwise there was no dealloying. So, if one has an alloy with 40 at.% silver and 60 at.% gold, one has to melt it with more silver so that the silver content exceeds about 55–60 at.%.

Dealloying is a major corrosion problem in industrial alloys—not so much in itself, but for its role in stress corrosion cracking. Dezincification of brass may have been noticed in Roman times, but the first scientific records date from the early 20th century, when this was a severe problem affecting α-brass seawater condenser tubes.[12] In this case, the parting limit is 20% Zn, a special case discussed later in this article. Bengough and May[13] systematized the addition of arsenic (in small amounts, less than 0.05 wt%) for resistance to macro-dezincification.

Historically, three types of mechanism have been proposed to explain how two elements, intermixed on an atomic scale, can be separated by electrolytic action. The most obvious is that the dissolution is not really selective at all, but that both elements dissolve, and then one replates. This cannot be occurring in the general case of dealloying because this often occurs at electrode potentials too low to oxidize the more-noble element, but it may be occurring, very locally, in the case of dezincification, where copper may be close to equilibrium with its soluble ions. The second mechanism, promoted by Pickering and Wagner,[14,15] involves divacancy injection and room-temperature lattice diffusion of these vacancies. This appears to be inconsistent with the rapid kinetics of dealloying, but as Pickering pointed out, it would account for the common observation of a significant residue of the less-noble metal in the dealloyed material. As well as graded solid-solution compositions, Pickering also observed intermediate phase formation in dealloyed ε-brass by x-ray diffraction[16] (this exact experiment was first reported in 1933).[17]

Recently, surface diffusion has been favored as the operative transport mechanism for the more-noble metal. Forty and others[18–21] made TEM observations of the early stages of porosity formation in silver-gold alloys immersed in nitric acid and developed a model for the parting limit based on surface diffusion and filling of incipient pores. This was not exactly an atomistic model but implied a balance between dissolution and surface diffusion that was developed by Sieradzki et al.[22] using atomistic Monte Carlo simulations of dealloying. These reproduced several main features, including parting limits, which were ascribed (not quite accurately in the case of the "55%" threshold) to site percolation thresholds in the lattice. Erlebacher[23] developed a much more sophisticated 3D simulation scheme, focusing mainly on morphology, kinetics, and potential dependence that forms the basis for secure comparisons with experiment.

Pickering made comprehensive studies of the electrode potential dependence of dealloying and the critical potential for dealloying (E_c). Up to E_c, the current density is low and almost potential-independent, and then it increases steeply at E_c,[15] as shown schematically in Figure 2. Uniform nanoporosity forms only above E_c, although Pickering often referred to "pitting," or localized porosity, below E_c.[24] As more gold is added to the alloy, E_c increases until, at the parting limit, only the flat, "passive" region is observed. Up to 30–40% gold, this behavior was reproduced, with good quantitative agreement with experiment by Erlebacher's simulations.[23] Then, a small refinement (prohibition of dissolution of atoms with 10 or 11 neighbors) reproduced the experimentally observed "55 at% Ag" parting limit almost exactly.[25] It was shown that this was close, but not identical, to a high-density percolation threshold for the lattice.[26]

Recently, there has been much discussion of the true value and meaning of E_c. In 1993, Sieradzki gave a model for E_c based on two effects—one thermodynamic (necessity of dissolving less-noble metal from very small clusters of atoms, thus creating a gold surface with very

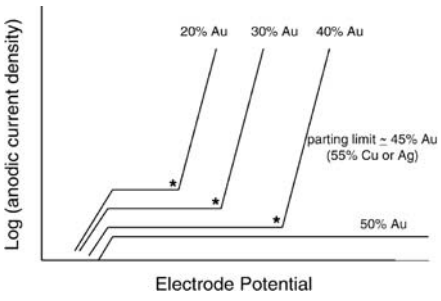

Figure 2. Schematic anodic dissolution behavior of a silver-gold or copper-gold alloy undergoing dealloying in a nonoxidizing aqueous acid, showing critical potentials for nanoporosity generation (*) and the inability to form nanoporosity when the silver or copper content falls below the parting limit, as indicated in the figure. (In practice, the flat current at 50% Au is succeeded eventually by gold oxidation or oxygen evolution.)

high curvature) and one kinetic (necessity of dissolving these atoms at a certain rate to avoid infilling by surface diffusion of gold).[27] More recently, it was proposed that an intrinsic critical potential can be identified, in simulation and experiment, that corresponds only to the thermodynamic (curvature) effect.[28,29]

Dealloying is more difficult (requires a higher potential) in ordered than in disordered CuAu.[30] This can be explained by considering the connectivity of less-noble metal atoms in the lattice. The disordered alloy has a cluster structure in which less-noble atoms comprising the dissolution path have many like neighbors, facilitating penetration of the electrolyte.

Ternary elements of low surface mobility alter the kinetics and product morphology. In the 1980s, it was suggested that the beneficial effect of arsenic in brass (on macro-dealloying, not stress corrosion cracking) was associated with the blocking of step edges, slowing down the surface diffusion of copper.[31,32] Lately, interest has turned to the addition of Pt. Kramer et al. demonstrated an enhanced specific surface area in nanoporous Au-Pt prepared from Ag-Cu-Au-Pt,[33] and Snyder et al. presented a systematic study of Ag-Au-Pt alloys, which show a refined porosity compared with Ag-Au.[34]

So why do some alloys show dealloying at the fcc site percolation threshold (20 at.%), while others require 55% of the less-noble element? The conditions for dezincification of α-brass are quite specific—corrosion has to proceed for some time (usually in an aerated chloride solution), and then dealloying starts under the resulting porous corrosion product—a well-established observation. Lucey[35,36] and later Newman et al.[31] gave different variants of the same explanation—there is an enrichment of copper ions (Lucey[35,36] referred to solid CuCl) under the corrosion product, and then the conditions closely approach equilibrium for the copper. Somehow this exchange enhances the mobility of copper, exposing more zinc for dissolution (but still respecting the site percolation threshold).

The role of dealloying in stress corrosion cracking (SCC) of bulk solid-solution alloys is an old discussion. For binary gold alloys, the correlation between the two is transparent,[37,38] especially with the recognition that local dealloying persists below the usually defined critical potential. The compositional dependences of dealloying and transgranular SCC in brass, exposed to a solution with which copper is equilibrated, are identical.[39] The actual mechanism of crack growth (and this may be different for inter-and transgranular SCC) remains controversial. According to Sieradzki and Newman,[40] both forms of SCC require only a thin dealloyed layer, which triggers a brittle substrate microcrack. Such crack jumps in fcc metals are impossible according to traditional mechanics, but evidence for the phenomenon has mounted, and it is especially easy to demonstrate for the intergranular variant in silver-gold alloys.[41–44]

Microstructure and Stability

Lattice Coherency

As Forty et al.[19] pointed out in the 1970s, the crystal lattice of the master alloy survives the dealloying, despite the small ligament size and topological complexity of the nanoporous product structure. This leads to a distinguishing feature of nanoporous metals: the grain size is much larger than the pore and ligament sizes. The long-range coherent crystal lattice is well confirmed by more recent studies using electron diffraction,[19,45] focused ion beam (FIB) microscopy,[46] high-resolution imaging in the TEM,[46] and electron backscatter diffraction images, such as the orientation map of Figure 1c.[47] For a nanoporous sample with a ligament size of 5 nm and grain size of 50 μm, each grain is a single crystal containing approximately 10^{12} nanoligaments.

Notwithstanding the previous results, there have been reports of a nanocrystalline nature of nanoporous gold (NPG), with its grain size similar to the ligament size.[48] It is not known to what extent the different structure reflects the specifics of the corrosion conditions or rather an effect of the preparation of electron-transparent samples on the structure.

Defect Structure

Typically, as-dealloyed nanoporous metals exhibit macrodefects in the form of cracks. Parida et al.[46] were the first to systematically investigate the large volume shrinkage (up to 30%) during dealloying, which is an obvious cause of the cracking. The shrinkage is largest for fast corrosion, that is, at high potentials in the case of potentiostatic dealloying. Such samples also contain many lattice defects, including dislocations, stacking faults, and twins, as detected by high-resolution (HR) TEM.[46] Electron tomography has also revealed closed voids in the solid phase.[49] Since there are comparatively few dislocations and faults in the master alloy and in NPG prepared by slow corrosion at a low dealloying potential, the lattice defects in the fast-dealloyed material must be generated during the dealloying. The lattice defects have been linked to plastic deformation in response to stress that arises from the capillary forces, as no macroscopic load is applied. The nature of this stress will be the subject of the next section of this article.

It is noteworthy that dislocations in nanoporous metals can be detected even if their core resides in the pore space rather than the solid phase. This is exemplified by the closure failure of Burgers circuits around most pores in nanoporous gold, as seen in HRTEM.[46] As Jin et al. pointed out,[47] the finding points toward "pore channel dislocations," with their cores located in the pore space, are somewhat similar to the dislocations with hollow cores that are observed in some complex oxides.[50]

The formation of cracks during dealloying may be suppressed by careful control of the corrosion process. Approaches include low potential electrochemical dealloying at an elevated temperature[47,51] and a multistep free corrosion procedure.[52] These approaches achieve a significant reduction in crack formation, although at the expense of forming a relatively large structure size. In fact, there has been no report so far on the successful fabrication of large (mm- or cm-sized), monolithic, and crack-free nanoporous metals or alloys with a structure size less than 10 nm. Developing such materials demands a better understanding of the dealloying process and the underlying volume shrinkage mechanisms. Since fundamental studies and possible applications will typically require high strength and/or high surface area, which both depend on small ligament size, more work on dealloying processes and on the underlying volume shrinkage mechanisms is required.

Coarsening

Owing to the large total excess surface energy, nanoporous structures are inherently unstable against coarsening. Severe coarsening was even observed at room temperature in NPG during electroless dealloying of Au-Ag alloys.[45] The coarsening process can be understood as curvature driven growth, where surface diffusion transports matter away from the convex regions—typically the necks at the center of the ligaments—with a positive-valued mean curvature, κ, toward concave regions of negative κ in the connecting nodes. The essential step in coarsening is thus the removal of ligaments when they pinch-off at their necks, quite analogous to the surface-tension driven disintegration of fluid cylinders by the Plateau-Raleigh instability.[53,54] The inner surface of nanoporous metals exhibits both concave and convex regions. The average value, $\langle\kappa\rangle$, of the mean curvature depends on the

solid fraction, φ. Studies using stereological analysis of 3D reconstructions based on electron tomography—such as Figure 1b—have found $\langle\kappa\rangle$ positive for more open nanoporous structures (smaller φ)[49] and near zero for denser ones.[55] This is not unexpected; if the two phases are interchanged in an arbitrary two-phase structure, maintaining the position of the interface, then φ and the local mean curvature values transform as $\varphi \to 1 - \varphi$ and $\kappa \to -\kappa$. Thus, the transition from more open to denser porous structures may invert the sign of $\langle\kappa\rangle$.

The coarsening of nanoporous solids is accelerated upon heating or immersion in concentrated acids.[56] Intriguingly, the porous structure remains self-similar, irrespective of the different length scales.[57] Strategies that have been devised to stabilize the nanoscale structure size or to form smaller structures include lowering the dealloying temperature[58] and the addition of a second noble element (e.g., Pt).[33,34] Surface oxidation during electrochemical dealloying is another effective and simple approach to prevent coarsening. Approximately one monolayer of superficial oxide is formed during potentiostatic dealloying of Ag-Au at a relatively high potential.[59] This results in very small and stable porous structure sizes, down to around 2 nm for NPG.[59] Consistent with the absence of coarsening, the structure size in this case is determined by the corrosion rate rather than by the total dealloying time, as in the corresponding free corrosion process. Free corrosion is a chemical process, typically in HNO_3 for Ag-Au, rather than the electrochemical one addressed earlier. Removal of the oxide layer—by cathodic sweep or exposure to a reducing agent such as CO (Reference 5)—triggers quasi instantaneous coarsening along with volume shrinkage.[59]

Mechanical Behavior: Scaling Laws

The mechanical integrity and reliability are critical in many applications of conventional porous materials, and generic relations coupling the properties to the porosity—as quantified here by the volume fraction, φ, of the solid—have been widely used in selecting and optimizing their microstructure.[60] Such "scaling equations" have been well established for materials with cell sizes of several micrometers and larger. Since the scaling equations do not depend on the structure size, and since the geometry—except for its length scale—does not fundamentally differ for nanoporous materials as compared to macroporous materials, one may use these equations as a starting point for inspecting nanoporous materials behavior.

The scaling equations ("Gibson-Ashby foam scaling equations") for the two most often reported mechanical properties, the effective macroscopic Young's modulus, Y, and the yield strength, σ_Y, are:[60]

$$Y = C_1 Y_B \varphi^2 \quad (1)$$

$$\sigma_Y = C_2 \sigma_{Y,B} \varphi^{3/2}, \quad (2)$$

where the subscript B refers to properties of massive samples of the solid bulk phase, and the C_i are constants with values that vary little for materials as dissimilar as sponge cake and foamed aluminum; specifically, $C_2 \approx 0.3$ for open cell foams with small solid fraction ($\varphi \le 0.3$).[60]

In view of the universal aspects of macroporous materials behavior, it is remarkable that nanoporous materials exhibit new phenomenology that is in fact *not* captured by the scaling equations, Equations 1 and 2. The deviations are all related to an emerging dependency of the materials behavior on the length scale set by the ligament or pore size. They enter the scene through at least three distinct size effects, to be exposed in more detail in the following sections. First, the elastic behavior of nanoporous metals reflects the action of capillary forces, which are irrelevant in macroporous materials. Second, the plastic behavior of the local building blocks, such as the ligaments in dealloyed nanoporous metals, differs from that of macroscopic matter. Third, the pore and ligament sizes can be dramatically different from the crystal size, so that many pores and ligaments in a nanoporous metal can be part of the same, coherent crystal lattice.

Elastic Deformation

For a material with a conventional microstructure, the canonical issue of elasticity is the reversible deformation in response to a load applied to the material's external surface. When applied to macroporous materials, the question relates to the elasticity of a heterogeneous medium consisting of the two phases (solid and pore) with different elastic responses. Nanoporous materials, on the other hand, impose an additional and quite different theme that is related to their many internal surfaces: What stress and strain is induced by the capillary forces acting locally, everywhere along the surfaces, and what are the ramifications for the material's behavior and stability? The issue leads right into the heart of a topic of 20th century thermodynamics that remains controversial even today,[61] namely the nature and origin of capillary forces at the surface of solids as opposed to fluids and the distinction between the surface tension, γ, and the surface stress, **s**. Topics arising in that context also include the question whether the crystal lattice can always support the stresses induced by the surface, the issue of a solid's elastic reaction to reversible changes in the capillary forces, and the issue of a possible impact of a modified stiffness of the matter at the surface on the material's macroscopic elastic response.

Capillary Forces: Surface Tension and Surface Stress

Since fluids do not support shear stress, the pressure, P, completely characterizes the stress state in their bulk. The Young-Laplace equation, $P = 2\kappa\gamma$, relates P in a droplet to γ and to the mean curvature, κ, of its surface. It reflects the energetics of a virtual compression of the droplet, which reduces the area, A, of the surface while leaving its atomic structure and, hence, γ unchanged. The variation in the total excess free energy due to the surface is $\delta F_S = \gamma\, \delta A$; this variation is governed by γ as the relevant capillary parameter. Since solid surfaces also exhibit surface tension, one might assume that the bulk of a solid also experiences a Laplace pressure. However, the fact that solids—contrary to fluids—support shear stress entails a fundamental distinction: in an elastic process, the surface layer of atoms strains here coherently with the underlying bulk crystal. This process leaves the number of atoms (and hence an appropriately measured surface area) invariant but changes the interatomic spacing. The free energy variation is then $\delta F_S = A\, \partial\gamma/\partial\mathbf{e}\, \delta\mathbf{e}$, with **e** being a tangential strain tensor and $\partial\gamma/\partial\mathbf{e} = \mathbf{s}$ being the surface stress tensor. The resulting balance equations are $\boldsymbol{\sigma} \cdot \mathbf{n} = \mathrm{div}_S\, \mathbf{s}$ locally[62] (where **n** and div_S denote the surface normal and the surface divergence operator, respectively) and

$$V \langle\boldsymbol{\sigma}\rangle_B + A \langle\mathbf{s}\rangle_S = 0 \quad (3)$$

for the average.[63] Here **σ** and V represent stress in the bulk and volume, respectively, and the brackets denote averages over bulk (B) or surface (S). Similar to the definition of the pressure in bulk as minus one third the trace of the stress tensor, it is common to define a scalar surface stress as $f = \frac{1}{2}$ trace **s**. In terms of this quantity, Equation 3 implies, in particular, that the mean pressure in the nanoporous solid obeys $3\, V \langle P\rangle_B = 2\, A \langle f\rangle_S$.

Mechanics thus imposes a fundamental distinction on the surface-induced stresses in solids, including nanoporous ones, as

opposed to fluids: the (Laplace-) pressure in a fluid scales with the surface tension, which has a positive value, and with the surface curvature, which can be of either sign. By contrast, there is never a Laplace pressure in solids. Instead (cf. Equation 3), the surface-induced pressure scales with the surface stress, which can be of either sign, and with area per volume, which is always positive. A discussion of common misconceptions regarding the distinction between the different capillary terms and their impact on materials behavior can be found in Reference 61.

In a microscopic picture, the surface tension relates to the fact that atoms at a surface—be it solid or fluid—exhibit an excess energy as compared to bulk, in the simplest case due to broken bonds. Surface stress, by contrast, represents the tendency of the surface atomic layer to favor a different interatomic spacing than the underlying bulk phase. In a solid, this leads to forces between the surface and the bulk. These forces have no equivalent in a fluid, since the surface atoms of the fluid can assume their preferred local arrangement at will, independent of the density in the underlying bulk liquid.

Lattice Instability at a Small Size

One more contrast to fluids and to Laplace pressure is that the surface-induced stress in the bulk of a solid depends on the orientation distribution of the surfaces and is, in general, anisotropic. For the example of a thin fiber—an idealized model of a ligament in a nanoporous material—with isotropic $\mathbf{s}$, the axial component of the surface-induced stress $\boldsymbol{\sigma}$ of Equation 3 is twice that of the radial component.[63] As a consequence, a shear stress acts in planes inclined to the fiber axis. This stress, which scales inversely with the fiber diameter, imposes a lower limit on the stable structure size: Fibers and, more generally, ligaments of dealloyed nanoporous materials undergo spontaneous shear when thinner than a around one or two nanometers.[64] The spontaneous collapse of ligaments by surface-induced shear is thought to drive the severe macroscopic shrinkage that is observed during dealloying at a high corrosion rate,[46] where ligament sizes can reach 2 nm and smaller. The surface-induced plastic deformation at a high corrosion rate is evidenced by the extreme number of lattice defects—dislocations and planar faults—as revealed by HRTEM on such samples.[46]

Charge-Induced Surface Stress and Actuation

While surface-induced stresses can be detrimental to the stability of extremely small objects, their consequences also can be beneficial when properly controlled. A prominent example is the reversible strain of nanoporous solids in response to reversible variation of their surface stress.[4,65] The underlying concept is that the properties of surfaces can be tuned by variation of the state variables in the surrounding medium, for instance, the electric or chemical potential in the fluid within the pore space. Figure 3c shows the variation in f, the surface stress (measured in a cantilever bending experiment with a single, planar electrode surface) of Au(111) in sulfuric acid electrolyte when the superficial charge density, q, is varied by cycling the electrode potential.[66] The linear response is apparent. In NPG, the variation of the surface-induced stress in the bulk, Equation 3, which reflects the variation in f, requires strain throughout the material. This leads to a cyclic macroscopic expansion and contraction (Figure 3a) that can be large enough to be visible with the naked eye, see Figure 3b. Nanoporous metals have thus been suggested as candidates for use as electrochemical actuators, with strain amplitudes and energy densities on par with ceramic or polymer actuator materials.[4] Very recently, the concept has been generalized to include large-strain actuation promoted by reversible, chemically driven changes in the surface stress.[5]

The linear response of the surface stress to surface charging provides another example of the fundamental difference between surface stress and surface tension. The Lippmann equation, a fundamental result of 19th century thermodynamics, shows that the surface tension varies quadratically with q. The comparison of the respective graphs in Figure 3c readily reveals the dramatic difference in the two distinct capillary forces. Yet another distinction is that $\gamma(q)$ is well understood and readily predicted by theory, whereas we still struggle to achieve a predictive understanding of the magnitude (empirically around –1 to –2 V for clean metal surfaces) and even of the sign of df/dq.[67]

Excess Elasticity

Besides being the source of bulk stress in the undeformed state of nanoscale materials, the surfaces may also affect the materials' elastic response. As the surface is strained, its surface stress value

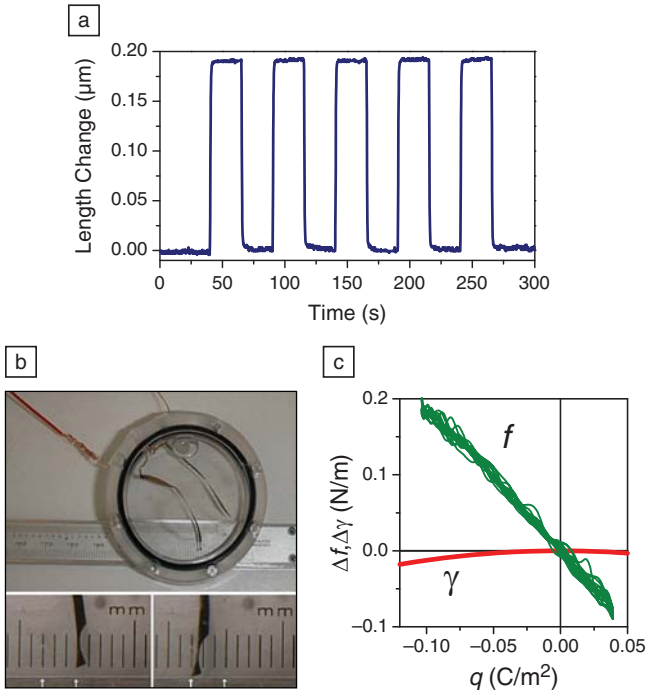

Figure 3. Reversible elastic deformation of nanoporous gold (NPG) induced by capillary forces. (a) Cyclic macroscopic length change of a mm-sized NPG sample when the electrode potential is varied with an amplitude of 1 V.[65] (b) Bimorph cantilever electrodes (massive gold foils that are coated on one side with NPG) exhibit cyclic strokes of several mm when the potential is varied.[65] White arrows mark various tip positions, illustrating the displacement. (c) Variation in surface stress f (green) and surface tension γ (red) with superficial charge density, q, during potential cycling. Note the distinctly different behavior of the two capillary parameters. Data in (c) is compiled from results in Reference 66.

changes, and so do the surface-induced stresses in the bulk. In other words, the surfaces may contribute to the elastic response, on top of the matter in the bulk. This behavior is the signature of an excess elasticity of the surface, for which the second derivative of the surface tension with respect to the tangential strain is the relevant parameter.[62] In the simplest case, namely isotropic surface stress, the relevant tangential strain variable is simply the relative change, e, in surface area by elastic strain. The relevant (scalar) excess elastic constant is then $\tau = \partial f/\partial e = \partial^2\gamma/\partial e^2$. Depending on their symmetry, real surfaces or interfaces may exhibit a vastly more complex behavior with many independent elastic parameters.[68] While the possible impact of surface elasticity on the effective macroscopic elastic response of nanoporous materials is appreciated in theory,[69] the experimental situation remains ambiguous. As can be seen in the compilation of Figure 4a, individual data sets for the elastic response of nanowires or for the ligaments in NPG may be taken as evidence for softening, stiffening, or no change at all when the size is decreased. Experiments on other materials with nanowire or similar geometry also disagree on the sign (i.e., softening or stiffening) of the surface excess modulus.[70–73] In Figure 4a, the results by Mathur and Erlebacher[74] stand out: The dramatically enhanced effective stiffness of their NPG samples at small ligament size may suggest a large, positive value of τ at the surface of gold.

An aspect that is separate in principle but that is in practice closely interconnected with that of the previous capillary effects is the dependency of the macroscopic elastic modulus of the porous material on its solid fraction φ (Equation 1). Here we are not looking at the consequences of surface behavior, but rather at softening due to the introduction of voids. This is a well-studied problem in mechanics (see, for instance, Reference 75), and scaling laws, such as Equation 1, often are found to be compatible with experimental results when excess elasticity is ignored (compare Figure 4a). In the instances where the theory fails to agree with experiment, it is not obvious to which degree failure should be blamed on inaccurate effective averaging over solid and void or to the neglect of surface excess elasticity.

Plastic Deformation

The plastic deformation behavior of nanoporous metals offers various fascinating aspects. The most obvious is that the ligament size can be adjusted to values well below 10 nm, possibly—as mentioned earlier—even down to the lower limit of stability for nanowires. Deformation tests on NPG will thus allow studies of nanowire strength to be extended down to sizes much smaller than what has been reached with individual wires. Furthermore, attempts to profit from the favorable mechanical behavior of nano-objects may require that many of them be assembled to obtain a strong macroscopic material. Nanoporous solids represent such materials, and their study probes deformation behavior of the assembly as well as the microscopic processes that act when many nano-objects deform in parallel. The existence of a quasi-macroscopic, coherent crystal lattice spanning the order of 10^{12} ligaments adds a new aspect to nanoporous metal

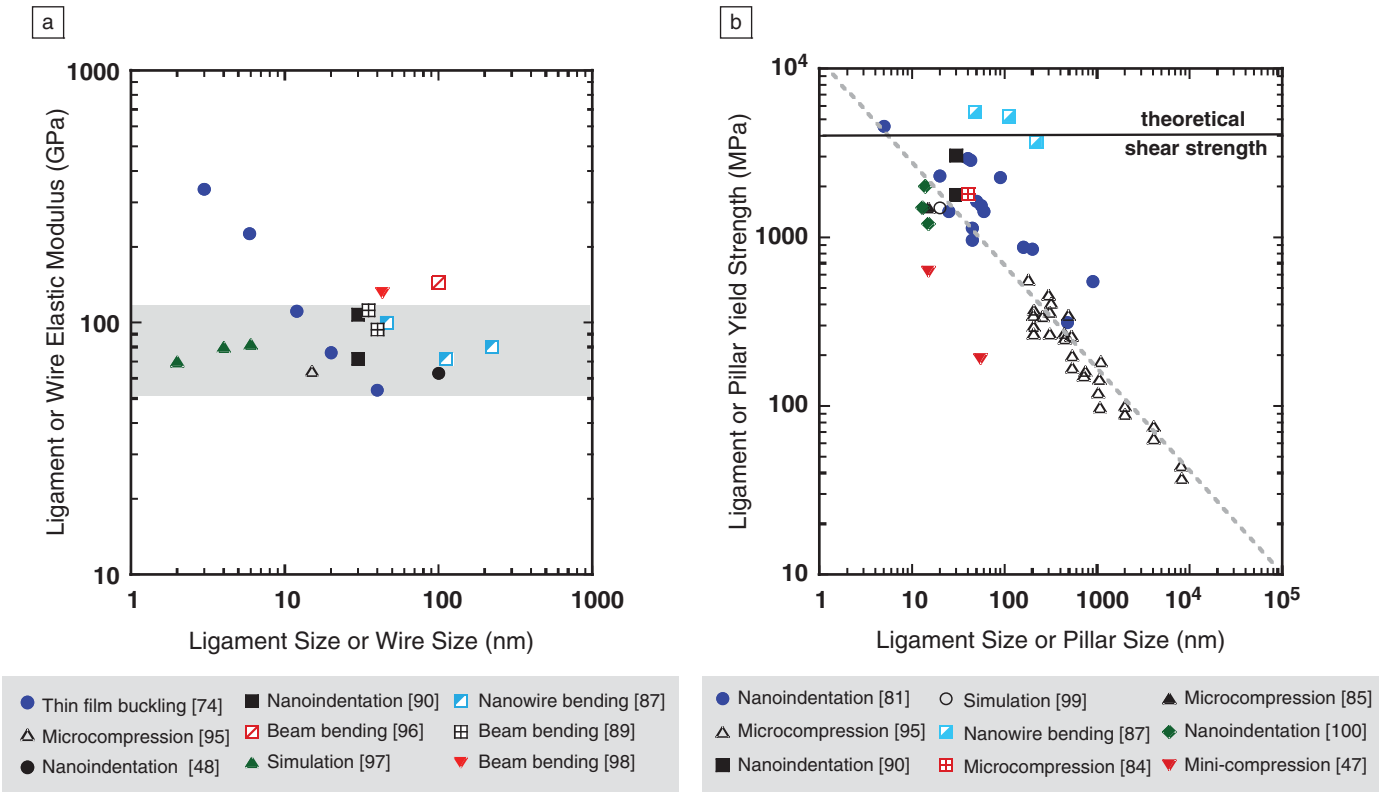

Figure 4. (a) Calculated ligament modulus and (b) yield strength of nanoporous gold as a function of the ligament diameter. Selected data for nanowires are also shown. Shaded area in (a) represents range of Young's modulus values for single-crystal gold in various crystallographic directions. In (b), the solid line denotes theoretical shear strength, and the dashed line is a power law with exponent –0.6. Data have been compiled from references indicated in the figure. Mini-compression stands for the compression of millimeter-sized samples (see also Figure 7).

deformation that has no equivalent in experiments on macroscopic foams or individual nanowires.

Li and Sieradzki[57] were the first to propose NPG as a model system for mechanical studies, and they focused on testing predictions on the ductile-brittle transition in random porous media by means of three-point bending tests on NPG beams. More recently, Biener et al.[48] introduced the use of instrumented nanoindentation for testing plastic yielding and flow of nanoporous materials. In the next sections, we shall describe recent results from nanoindentation, compression, and tensile tests and how the results affect our understanding of nanoporous metal plasticity. We shall also comment on emerging strategies for toughening of nanoporous metals.

Indentation Tests

Indentation as a tool to measure hardness on macro-size foams is well documented in the literature,[76–80] and the data analysis procedures have been transferred to the nanoindentation tests. The main issue regarding foam indentation is an assumption on the relation between indentation hardness, H, and the yield stress, σ_Y, as discussed by Hodge et al.[81] Macroscopic foams typically behave as fully compressible materials, in other words, the compression is entirely converted into densification, and the amount of transverse plastic strain that accompanies the longitudinal plastic compression—as characterized by the ratio of the two quantities, the "plastic Poisson ratio" ν_P—is ideally zero.[82,83] In indentation studies, one finds $H \sim \sigma_Y$, notwithstanding the more familiar $H \sim 3\ \sigma_Y$, of a massive (i.e., nonporous) material. In fact, low-density nanoporous metal indentation has been shown to be mostly plastic, and thus mostly compressible; regions outside the indent remain undeformed, as seen in Figure 5.[84] Recent compression tests on millimeter-sized samples of NPG (compare later in text) provide a more direct confirmation of this observation, with near-zero values of ν_P up to large compressive strain.[47] Yet, the picture is not unanimously supported; the micropillar compression tests of Reference 85 expose "barreling," that is, a squeezing out of the sides when the pillar is compressed. This implies a nonzero value (around 0.2) of ν_P. The origin of the discrepancy has not been resolved.

Micropillar Compression Tests

In principle, compression tests under uniaxial load afford a more straightforward analysis of the constitutive behavior of nanoporous metals, avoiding the assumptions on their hardness-yield strength relation that are required for indentation test analysis. Yet, the crack-free, macroscopic samples of nanoporous materials that would be required for such tests have been notoriously difficult to prepare. This has stimulated the use of miniaturized samples of NPG, such as the FIB–machined micropillars studied by Volkert et al. (Figure 6), with sizes on the order of a few microns.[85] These samples exhibit ductile plastic deformation up to true strains of around 30%. While their macroscopic yield strength is of the order of 100 MPa, use of the Gibson-Ashby foam scaling law, Equation 2, suggests that the local yield strength of the ligaments is extremely high: At 1.5 GPa (for ligament diameter L = 15 nm), its value is close to the theoretical strength of Au. Yet, recent investigations suggest that exposure of NPG to the FIB—even during the short durations required for imaging rather than machining—may lead to cracking along grain boundaries and to ligament coarsening.[86] This observation suggests that FIB-machining may modify the mechanical behavior, and it motivates tests on macroscopic samples in their as-dealloyed state, free of possible artifacts from machining.

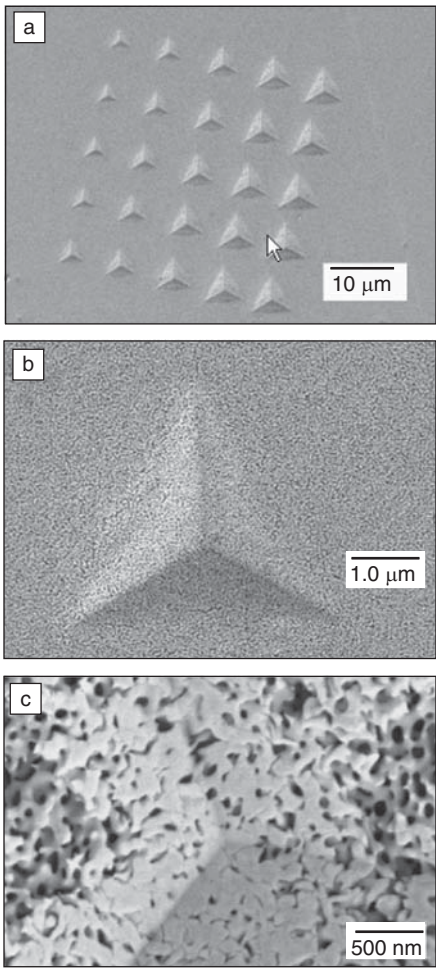

Figure 5. Scanning electron micrographs of nanoindentation on a fractured surface of nanoporous gold with Berkovich tip with a curvature of ~200 nm.[84] (a) typical nanoindentation array, (b) increased magnification of a single indent, and (c) zoom in of Figure 5b. Note that the plastic deformation is confined to the area under the indenter, and adjacent areas are virtually undisturbed.

Compression Tests on Macroscopic Samples

As was mentioned previously, conventional dealloying conditions produce cracks; this impairs mechanical tests of macroscopic samples. By slowing down the corrosion rate and enhancing the dealloying temperatures, Senior and Newman[51] obtained crack-free NPG sheets that exhibited appreciable elastic bending stretch, albeit only in a "wet" state with the pores filled with electrolyte. Using a similar strategy, Jin et al. successfully prepared millimeter-sized NPG samples, which were free of cracks and

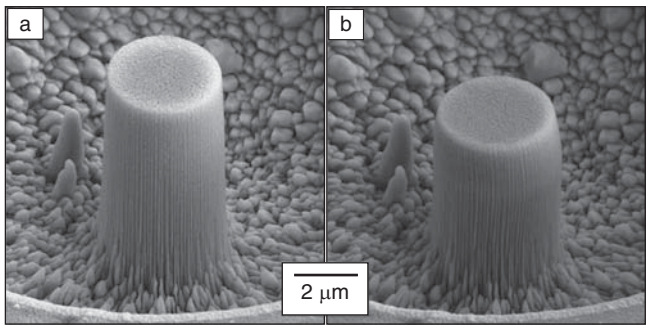

Figure 6. Focused ion beam machined nanoporous Au column with an initial diameter of 3.6 μm and height of 6.9 μm (a) before and (b) after compression to 22% strain.[85]

ductile in compression even in their "dry" state.[47] Results from such tests, as shown in Figures 4b and 7 as "mini-compression," do not support all findings from indentation and micropillar experiments, as already mentioned in relation to the plastic Poisson ratio. Most importantly, the macroscopic samples exhibit remarkably low yield strength. For instance, σ_Y = 7.5 MPa is found for NPG with a 55 nm ligament diameter and 25% density. The ligament yield strength inferred from Equation 2 for this sample is 190 MPa, more than one order of magnitude smaller than that of freestanding nanowires (e.g., 3.5 GPa for 100 nm diameter nanowire[87]). An equally interesting finding is that the mm-sized samples deform homogeneously, as indicated by electron backscatter diffraction images recorded throughout the deformation.[47] By contrast, conventional low-density foam materials exhibit a highly nonuniform deformation, carried by localized "crushing" or "densification" bands.[88] The large and uniform plastic strain opens up opportunities for inspecting previously unexplored aspects of nanoporous materials and nano-objects. For instance, strain rate jump tests have been carried out, revealing a near-zero strain rate sensitivity in the initial stages of deformation of NPG.[47]

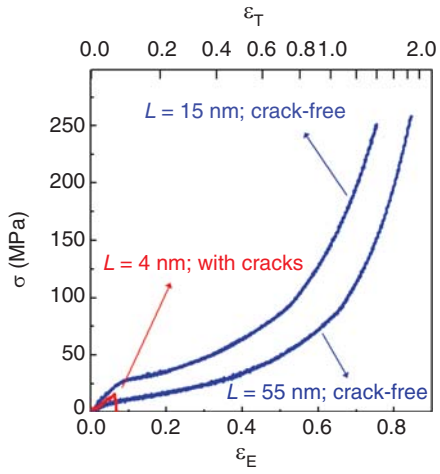

Figure 7. Compression stress-strain curves of nanoporous gold (NPG) samples with dimension of 1 × 1 × 2 mm^3 (mini-compression). Conventionally prepared NPG samples, containing preformed cracks, fracture in the elastic region (red). Crack-free samples (blue) are plastic in compression.[47] *L* refers to the ligament diameter. ε_E and ε_T represent the engineering strain and the true strain, respectively. σ is the true stress. Here, the engineering stress and true stress are approximately identical because of the negligible transverse strain during compression.

Nanoporous Layers—Tensile Tests

Experiments to determine the elastic and plastic properties of nanoporous metals by nanoindentation and micropillar tests induce a compressive stress state in the material. Indeed, as plastic deformation proceeds in such methods, the nanoporous metal becomes more compact, which complicates interpretation of the results. Other experiments have been performed in which the stress state is one of predominantly tension. These experiments, using the deflection of freestanding beams of NPG in response to loading with a nanoindenter, avoid some of the said complications.

Seker et al.[89] completed one such set of experiments in which NPG films were deposited onto a substrate, and freestanding beams were fabricated by a dealloying, thermal annealing, and FIB regimen. Lee et al.[90,91] conducted a second set of experiments (Figure 8) in which double-clamped beams of NPG were fabricated from commercially available gold-silver alloy leaf and appropriately processed by electron beam lithographic techniques. For details on NPG preparation based on gold leaf, see Reference 45.

The elastic stiffness of the specimens by Seker et al.[89] ranged from about 12 GPa to 18 GPa for solid fraction, φ, between 0.28 and 0.20, and the maximum deflection of the specimens was approximately the thickness of the beam. On the other hand, the elastic stiffness obtained by Lee et al.[90,91] was about 9 GPa for φ = 0.35. Further, the deflections of the beams at failure were between four and five times the beam thickness, so the force-displacement relationship was decidedly nonlinear due to finite deformation kinematics. Therefore, both types of specimens were predominantly in tension during the test. Both sets of specimens failed in what would typically be described as a brittle mode. There was strong evidence, however, that plastic deformation occurred in individual ligaments. This resulted in highly localized deformation, which rapidly propagated across the beam. The average stress in the films at failure in the Lee et al.[90,91] films was between 76 MPa and 111 MPa, which corresponds to a ligament stress of up to 1.45 GPa based upon Equation 2.

Scaling of Plastic Behavior

Upon inspecting the implications of the previous experiments for the mechanical behavior of NPG, which is the most-studied nanoporous metal,[48,74,81,85,90,92] it was found that effective values of the macroscopic yield strength range from 15 to 240 MPa.[93] If it is assumed that σ_{YB} = 200 MPa for massive Au and that solid fractions ranged from 0.25 to 0.42, the

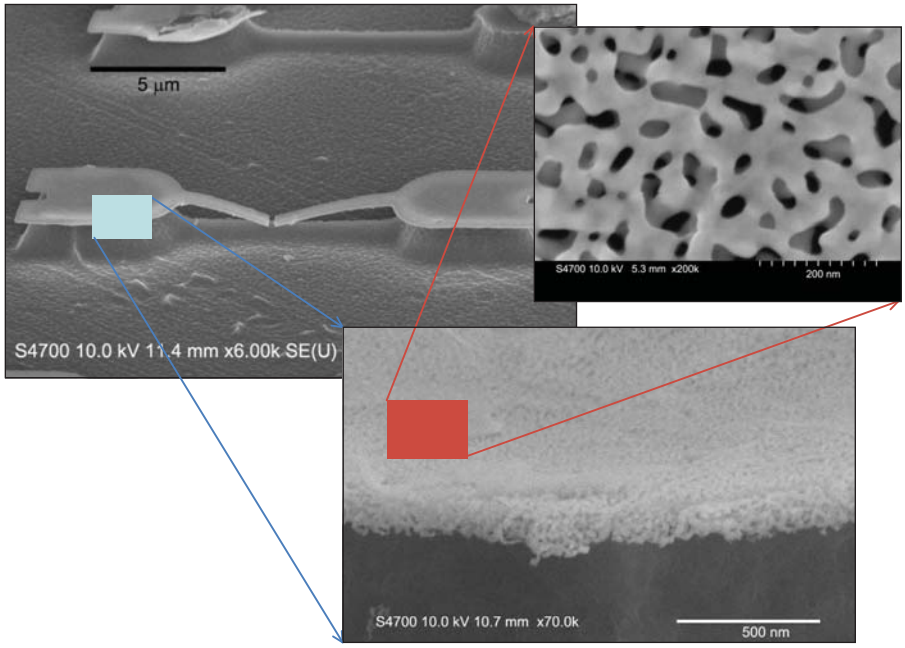

Figure 8. Nanoporous gold double-clamped beam with a thickness of 100 nm tested to mechanical failure by nanoindentation. (Images courtesy of Dr. Dongyun Lee at the Department of Nanomaterials Engineering, Pusan National University, Korea.)

macroscopic yield strength values from 7.5 to 16 MPa are predicted using Equation 2. This clearly disagrees with experiment: the actual yield strength of NPG is higher than predicted, sometimes by more than an order of magnitude.[48] The disagreement is resolved when one acknowledges the separate scaling law that links the yield strength of nanowires to their diameter.[85] In other words, the bulk yield strength value, $\sigma_{Y,B}$, in Equation 2 exhibits a size dependence, for which power laws of the form

$$\sigma_{Y,B} \propto L^m \quad (4)$$

are proposed, with m as an empirical exponent. A Hall-Petch–type $L^{-1/2}$ law[81] or a somewhat steeper (about $L^{-0.6}$, Reference 85) size dependence has been suggested.

Figure 4b compiles experimental results for σ_Y from a wider range of sample types, showing reasonable agreement with the $L^{-0.6}$ law, though with significant scatter.[93] Remarkably, however, the results obtained from the compression tests on quasi-macroscopic NPG (the test on mm-sized samples labeled "mini-compression" in Figure 4b) indicate systematically and significantly (by at least the factor three) lesser yield strength. These results also identify the functional relationship between indentation hardness and yield strength as an issue that requires more study. Along with the scatter that is apparent in the data of Figure 4b, the results suggest that other nanoporous metals systems may need to be tested for more reliable statements, and an improved understanding of the deformation mechanisms at the nanoscale is needed.

Microscopic Aspects

As stated previously, the scaling of nanoporous metal yield strength with ligament size is being linked to an analogous scaling in nanowires. The underlying notion is that the deformation of ligaments is controlled by the same microscopic phenomena as that of nanowires, for instance, dislocation nucleation and egression at free surfaces. Yet, this approach ignores a distinguishing feature of nanoporous metals, namely the coherent crystal lattice that extends over scales much larger than the ligament size. In fact, each grain in the polycrystalline microstructure of Figure 1 contains billions of nanoligaments with a common, coherent lattice structure and, therefore, a common set of crystallographic slip planes. Lattice dislocations can be defined in such a nanoporous crystal. Since they can extend and move over distances much larger than the ligament diameter, the deformation acquires a coherent character that has no analogy in nanowire plasticity.[47]

An intriguing aspect of the defect structure of nanoporous metals is the pore channel dislocations, addressed earlier in this article. Yielding of an individual ligament via shear by one Burgers vector creates a pore-channel dislocation loop surrounding it and associated long-range stress and strain fields that favor the coordinated propagation of slip—in the neighboring ligaments—on the same set of glide planes. Here again, it must be concluded that the deformation and failure of nanoporous metals reflects coupled deformation processes of many ligaments, rather than uncorrelated local yielding.

Toughening Strategies

So far, our discussion has focused on single-phase, single-component nanoporous metals that attract attention as simple model systems for studying elastic and plastic behavior at the lower end of the structure size scale, with an eye on future, high-strength nanomaterials. For applications, on the other hand, one is interested in macroscopic mechanical performance, irrespective of the complexity of the system. Any material of interest will need to combine strength and toughness. Central issues then are not so much the strengthening of individual ligaments at the nanoscale, but rather the prevention of native crack formation by control of the dealloying process (see subsection of this article on "Defect Structure") and the arrest of propagating cracks—possibly at a mesoscopic length scale—as well as the prevention of coarsening.

The first nanoporous metal with appreciable toughness in macroscopic size samples was achieved by incorporation of a dendritic second phase as a crack arrester, a toughening strategy that had been widely used for other brittle materials such as ceramics or metallic glasses. Jin et al.[94] started with a Pt-Ag master alloy that decomposed into two phases during solidification: a Ag-rich solid-solution [Ag] matrix phase with Pt content below the parting limit and Pt-rich solid-solution [Pt] dendrites above the parting limit. Dealloying transforms the [Ag] phase into nanoporous Pt. The [Pt] dendrites, being stable against corrosion, remain unaffected. In this way, one obtains a macroscopic composite material with micron-size, massive dendrites embedded in a nanoporous Pt matrix. The material exhibits a ligament diameter less than 5 nm, an appreciable volume-specific surface area (9×10^5 cm^{-1}), and yield strength as high as 250 MPa, as measured by compression tests on millimeter-sized samples.[94]

Outlook

Many significant issues are still open for future research in the field of nanoporous metal formation and mechanical behavior. Some of the opportunities include

- Applications as well as fundamental research to develop schemes for fabricating crack-free nanoporous metals with macroscopic sample size and, at the same time, ligaments with extremely small diameters, below 5 nm.
- Determining the role of dealloying and of nanoporous layers in stress corrosion cracking. In turn, there could be devices, involving partially dealloyed materials, where such a phenomenon would constitute a degradation or failure mode for the device.
- The distinctly different nature of the capillary forces at the surface of a (nanoporous) solid as opposed to a fluid. The problem extends to the balance of these forces with the stresses in the bulk, which is often—and erroneously—discussed in terms of the Laplace equation.
- The origin of the large apparent deviation of the effective elastic constants of nanoporous metal at very small ligament size. Can we obtain reproducible values for the sign and possibly the magnitude of the surface excess elastic constants that are under discussion as a possible origin?
- The reduction of mechanical behavior of nanoporous metals to a combination of the two scaling laws: Equations 2 and 4. In other words, can the deformation be understood as the uncorrelated yielding of ligaments that behave individually as isolated nanowires? Alternatively, how relevant are collective effects mediated by the long-range coherent crystal lattice?
- The origin of the discrepancy between the yield-strength values obtained with the different testing schemes, such as nanoindentation and micropillar testing, and (quasi) macroscopic compression experiments should be determined.

Along with the prospects of use in applications—some of which are being discussed in other articles in this issue—the open issues may be viewed as a stimulus for ongoing research into nanoporous metals and the processes that underlie their formation and mechanical performance.

Acknowledgment

JWK is grateful to the National Science Foundation CMMI-0826093 for support.

References

1. J. Rouquerol, D. Avnir, C.W. Fairbridge, *Pure Appl. Chem*. **66**, 1739 (1994).
2. J. Erlebacher, M.J. Aziz, A. Karma, N. Dimitrov, K. Sieradzki, *Nature* **410**, 450 (2001).
3. H. Gleiter, J. Weissmüller, O. Wollersheim, R. Würschum, *Acta Mater*. **49**, 737 (2001).
4. J. Weissmüller, R.N. Viswanath, D. Kramer, P. Zimmer, R. Würschum, H. Gleiter, *Science* **300**, 312 (2003).
5. J. Biener, A. Wittstock, L. Zepeda-Ruiz, M.M. Biener, D. Kramer, R.N. Viswanath, J. Weissmüller, M. Bäumer, A.V. Hamza, *Nat. Mater*. **8**, 47 (2009).
6. M. Sagmeister, U. Brossmann, S. Landgraf, R. Würschum, *Phys. Rev. Lett*. **96**, 156601 (2006).
7. S. Dasgupta, S. Gottschalk, R. Kruk, H. Hahn, *Nanotechnology* **19**, 435203 (2008).
8. H. Drings, R.N. Viswanath, D. Kramer, C. Lemier, J. Weissmüller, R. Würschum, *Appl. Phys. Lett*. **88**, 253103 (2006).
9. S. Ghosh, C. Lemier, J. Weissmüller, *IEEE Trans. Magn*. **42**, 3617 (2006).
10. L. Reti, *Isis* **56**, 307 (1965).
11. J. Seath, F.E. Beamish, *Ind. Eng. Chem., Anal. Ed*. **10**, 639 (1938).
12. G.D. Bengough, *J. Inst. Met*. **27**, 51 (1922).
13. G.D. Bengough, R. May, *J. Inst. Met*. **32**, 81 (1924).
14. H.W. Pickering, C. Wagner, *J. Electrochem. Soc*. **114**, 698 (1967).
15. H.W. Pickering, Y.S. Kim, *Corros. Sci*. **22**, 621 (1982).
16. H.W. Pickering, *J. Electrochem. Soc*. **117**, 8 (1970).
17. C.W. Stillwell, E.S. Turnipseed, *Phys. A* **4**, 263 (1933).
18. A.J. Forty, *Nature* **282**, 597 (1979).
19. A.J. Forty, P. Durkin, *Philos. Mag. A* **42**, 295 (1980).
20. A.J. Forty, G. Rowlands, *Philos. Mag. A* **43**, 171 (1981).
21. P. Durkin, A.J. Forty, *Philos. Mag. A* **45**, 95 (1982).
22. K. Sieradzki, R.R. Corderman, K. Shukla, R.C. Newman, *Philos. Mag. A* **59**, 713 (1989).
23. J. Erlebacher, *J. Electrochem. Soc*. **151**, C614 (2004).
24. J.D. Fritz, H.W. Pickering, *J. Electrochem. Soc*. **138**, 3209 (1991).
25. D.M. Artymowicz, R.C. Newman, J.D. Erlebacher, *Electrochem. Soc. Trans*. **3** (31), 499 (2006).
26. D.M. Artymowicz, R.C. Newman, J.D. Erlebacher, *Philos. Mag*. (2009), in press.
27. K. Sieradzki, *J. Electrochem. Soc*. **140**, 2868 (1993).
28. J. Rugolo, J. Erlebacher, K. Sieradzki, *Nat. Mater*. **5**, 946 (2006).
29. A. Dursun, D.V. Pugh, S.G. Corcoran, *Electrochem. Solid State Lett*. **6**, B32 (2003).
30. B.W. Parks, J.D. Fritz, H.W. Pickering, *Scripta Metall*. **23**, 951 (1989).
31. R.C. Newman, T. Shahrabi, K. Sieradzki, *Corros. Sci*. **28**, 873 (1988).
32. R.C. Newman, *Corros. Sci*. **33**, 1653 (1992).
33. D. Kramer, R.N. Viswanath, S. Parida, J. Weissmüller, *Mater. Res. Soc. Symp. Proc*. **876E**, R2.5 (2005).
34. J. Snyder, P. Asanithi, A.B. Dalton, J. Erlebacher, *Adv. Mater*. **20** (10), 1876 (2008).
35. V.F. Lucey, *Br. Corros. J*. **1**, 9 (1965).
36. V.F. Lucey, *Br. Corros. J*. **1**, 53 (1965).
37. H.W. Pickering, *Corrosion* **25**, 289 (1969).
38. D. Gorse, A. Legris, J.L. Pastol, B. Maiki, *J. Electrochem. Soc*. **146**, 3702 (1999).
39. K. Sieradzki, J.S. Kim, A.T. Cole, R.C. Newman, *J. Electrochem. Soc*. **134**, 1635 (1987).
40. K. Sieradzki, R.C. Newman, *J. Phys. Chem. Solids* **48**, 1101 (1987).
41. R.G. Kelly, A.J. Frost, T. Shahrabi, R.C. Newman, *Metall. Trans. A* **22A**, 531 (1991).
42. M. Saito, G.S. Smith, R.C. Newman, *Corros. Sci*. **35**, 411 (1993).
43. F. Friedersdorf, K. Sieradzki, *Corrosion* **52**, 331 (1996).
44. A. Barnes, N.A. Senior, R.C. Newman, *Metall. Trans. A* (2009), in press.
45. Y. Ding, Y.-J. Kim, J. Erlebacher, *Adv. Mater*. **16**, 1897 (2004).
46. S. Parida, D. Kramer, C.A. Volkert, H. Rösner, J. Erlebacher, J. Weissmüller, *Phys. Rev. Lett*. **97**, 035504 (2006).
47. H.J. Jin, L. Kurmanaeva, J. Schmauch, H. Rösner, Y. Ivanisenko, J. Weissmüller, *Acta Mater*. 57, 2665 (2009).
48. J. Biener, A.M. Hodge, A.V. Hamza, L.M. Hsiung, J.H. Satcher, *J. Appl. Phys*. **97**, 024301 (2005).
49. H. Rösner, S. Parida, D. Kramer, C.A. Volkert, J. Weissmüller, *Adv. Eng. Mater*. **9**, 535 (2007).
50. J.P. Hirth, D.J. Srolovitz, *Philos. Mag. A* **69**, 341 (1994).
51. N.A. Senior, R.C. Newman, *Nanotechnology* **17**, 2311 (2006).
52. Y. Sun, K.P. Kucera, S.A. Burger, T.J. Balk, *Scripta Mater*. **58**, 1018 (2008).
53. J. Plateau, *Statique expérimentale et théorique des liquides soumis aux seules forces moléculaires* (Gauthier-Villars, Paris, 1873).
54. J.W. Strutt (Lord Rayleigh), *Philos. Mag*. **34**, 145 (1892).
55. T. Fujita, L.H. Qian, K. Inoke, J. Erlebacher, M.W. Chen, *Appl. Phys. Lett*. **92**, 251902 (2008).
56. M. Hakamada, M. Mabuchi, *Nano Lett*. **6**, 882 (2006).
57. R. Li, K. Sieradzki, *Phys. Rev. Lett*. **68**, 1168 (1992).
58. L.H. Qian, M.W. Chen, *Appl. Phys. Lett*. **91**, 083105 (2007).
59. H.J. Jin, S. Parida, D. Kramer, J. Weissmüller, *Surf. Sci*. **602**, 3588 (2008).
60. L.J. Gibson, M.F. Ashby, *Cellular Solids: Structure and Properties* (Cambridge University Press, UK, 1997).
61. D. Kramer, J. Weissmüller, *Surf. Sci*. **601**, 3042 (2007).
62. M.E. Gurtin, A.I. Murdoch, *Arch. Ration. Mech. Anal*. **57**, 291 (1975).
63. J. Weissmüller, J.W. Cahn, *Acta Mater*. **45**, 1899 (1997).
64. J. Diao, K. Gall, M.L. Dunn, *Nat. Mater*. **2**, 656 (2003).
65. D. Kramer, R.N. Viswanath, J. Weissmüller, *Nano Lett*. **4**, 793 (2004).
66. M. Smetanin, R.N. Viswanath, D. Kramer, D. Beckmann, T. Koch, L. Kibler, D.M. Kolb, J. Weissmüller, *Langmuir* **24**, 8561 (2008).
67. F. Weigend, F. Evers, J. Weissmüller, *Small* **2**, 1497 (2006).
68. M.E. Gurtin, J. Weissmüller, F. Larché, *Philos. Mag. A* **78**, 1093 (1998).
69. H.L. Duan, J. Wang, Z.P. Huang, B.L. Karihaloo, *J. Mech. Phys. Solids* **53**, 1574 (2005).
70. G.Y. Jing, H.L. Duan, X.M. Sun, Z.S. Zhang. J. Xu, Y.D. Li, J.X. Wang, D.P. Yu, *Phys. Rev. B* **73**, 235409 (2006).
71. S. Cuenot, C. Fretigny, S. Demoustier-Champagne, B. Nysten, *Phys. Rev. B* **69**, 165410 (2004).
72. S.G. Nilsson, X. Borrise, L. Montelius, *Appl. Phys. Lett*. **85**, 3555 (2004).
73. X.X. Li, T. Ono, Y.L. Wang, M. Esashi, *Appl. Phys. Lett*. **83**, 3081 (2003).
74. A. Mathur, J. Erlebacher, *Appl. Phys. Lett*. **90**, 061910 (2007).
75. C.-W. Nan, *Progr. Mater. Sci*. **37**, 1 (1993).
76. E.W. Andrews, G. Gioux, P. Onck, L.J. Gibson, *Int. J. Mech. Sci*. **43**, 701 (2001).
77. Z. Liu, C.S.L. Chuah, M.G. Scanlon, *Acta Mater*. **51**, 365 (2003).
78. U. Ramamurty, M.C. Kumaran, *Acta Mater*. **52**, 181 (2004).
79. Y. Toivola, A. Stein, R.F. Cook, *J. Mater. Res*. **19**, 260 (2004).
80. M. Wilsea, K.L. Johnson, M.F. Ashby, *Int. J. Mech. Sci*. **17**, 457 (1975).
81. A.M. Hodge, J. Biener, J.R. Hayes, P.M. Bythrow, C.A. Volkert, A.V. Hamza, *Acta Mater*. **55**, 1343 (2007).
82. G. Gioux, T.M. McCormack, L.J. Gibson, *Int. J. Mech. Sci*. **42**, 1097 (2000).
83. R.E. Miller, *Int. J. Mech. Sci*. **42**, 729 (2000).
84. J. Biener, A.M. Hodge, J.R. Hayes, C.A. Volkert, L.A. Zepeda-Ruiz, A.V. Hamza, F.F. Abraham, *Nano Lett*. **6**, 2379 (2006).
85. C.A. Volkert, E.T. Lilleodden, D. Kramer, J. Weissmüller, *Appl. Phys. Lett*. **89**, 061920 (2006).
86. Y. Sun, T.J. Balk, *Scripta Mater*. **58**, 727 (2008).
87. B. Wu, A. Heidelberg, J.J. Boland, *Nat. Mater*. **4**, 525 (2005).
88. A.E. Simone, L.J. Gibson, *Acta Mater*. **46**, 3109 (1998).
89. E. Seker, J.T. Gaskins, H. Bart-Smith, J. Zhu, M.L. Reed, G. Zangari, R. Kelly, M.R. Begley, *Acta Mater*. **55** (14), 4593 (2007).
90. D. Lee, X. Wei, X. Chen, M. Zhao, S.C. Jun, J. Hone, E.G. Herbert, W.C. Oliver, J.W. Kysar, *Scripta Mater*. **56** (5), 437 (2007).
91. D. Lee, X.D. Wei, M.H. Zhao, X. Chen, S.C. Jun, J. Hone, J.W. Kysar, *Modell. Simul. Mater. Sci. Eng*. **15** (1), S181 (2007).
92. M. Hakamada, M. Mabuchi, *Scripta Mater*. **56**, 1003 (2007).
93. J. Biener, A.M. Hodge, A.V. Hamza, in *Micro and Nano Mechanical Testing of Materials and Devices*, F. Yang, J.C.M. Li, Eds. (Springer, New York, 2008), p. 121.
94. H.J. Jin, D. Kramer, Y. Ivanisenko, J. Weissmüller, *Adv. Eng. Mater*. **9**, 849 (2007).
95. C.A. Volkert, E.T. Lilleodden, *Philos. Mag*. **86**, 5567 (2006).
96. R.C. Newman, S.G. Corcoran, J. Erlebacher, M.J. Aziz, K. Sieradzki, *MRS Bull*. **24** (7), 24 (1999).
97. S.J.A. Koh, H.P. Lee, *Nanotechnology* **17**, 3451 (2006).
98. E. Seker, J.T. Gaskins, H. Bart-Smith, J. Zhu, M.L. Reed, G. Zangari, R. Kelly, M.R. Begley, *Acta Mater*. **56**, 324 (2008).
99. L.A. Zepeda-Ruiz, B. Sadigh, J. Biener, A.M. Hodge, A.V. Hamza, *Appl. Phys. Lett*. **91**, 101907 (2007).
100. Y. Sun, J. Ye, Z. Shan, A.M. Minor, T.J. Balk, *JOM* **59**, 54 (2007). □